Chemical Science

ROYAL SOCIETY OF CHEMISTRY

EDGE ARTICLE

View Article Online
View Journal | View Issue

Open Access Article. Published on 29 August 2025. Downloaded on 10/28/2025 1:59:05 PM.
This article is licensed under a Creative Commons Attribution-NonCommercial 3.0 Unported Licence.

Check for updates

Cite this: *Chem. Sci.*, 2025, **16**, 17820

All publication charges for this article have been paid for by the Royal Society of Chemistry

Regioselective photodimerization as a tool for light-regulated catalyst assembly

Tommaso Marchetti, Federico Rastrelli, Maohua Lin, Alessandro Negri, Sara Bonacchi, Leonard J. Prins and Luca Gabrielli *

Received 27th May 2025
Accepted 14th August 2025

DOI: 10.1039/d5sc03858h

rsc.li/chemical-science

While photoisomerization has dominated the design of photoswitchable catalysts, this work introduces an alternative approach: leveraging light-induced photodimerization to assemble catalytically active species. The adopted strategy is based on a acrylamidylpyrene derivative equipped with a TACN·Zn(II) catalytic unit. This system undergoes a visible-light-induced [2 + 2] cycloaddition, which is both regioselective and reversible, to form a catalytically active photodimer. While the *E*-to-*Z* photoisomerization of the monomer has no significant effect on catalysis, the photodimerization leads to a six-fold enhancement in catalytic activity. The photodimer's catalytic efficiency is attributed to the clustering of catalytic units, facilitating a more efficient transphosphorylation reaction. Notably, this system demonstrates the ability to temporally control catalytic reactivity, as the active dimer can be reverted to the monomers upon irradiation with UV light. This work highlights the potential of photodimerization as a robust alternative strategy for regulating catalytic activity and opens new avenues for light-responsive catalysis with temporal control.

Introduction

Photoresponsive systems that couple catalytic function to light stimuli play a central role in fundamental biological processes, such as vision,[1,2] light-directed growth and movement in plants.[3] Additionally, plants leverage the conversion of light energy into chemical bonds to activate proteins *via* photodimerization,[4] a process that is fundamental for regulating gene expression, circadian rhythms, and photomorphogenesis.[5–7] Chemists have harnessed light to regulate catalytic activity, primarily exploiting photoisomerization processes to alter the geometry or electronic properties of catalyst architectures.[8] Azobenzene scaffolds, for instance, have been widely explored to achieve photoswitchable catalysis by exploiting cooperative,[9–17] electronic,[18–21] or steric effects,[22–25] or by inducing the self-assembly of molecules into supramolecular structures.[26–28] Similarly, light-driven isomerization of molecular rotors[29–31] and ring-closing/ring-opening reactions of photoactive dithienylethene[32–35] and spiropyran[36] derivatives have been employed to design light-responsive catalysts.

In this work, we present an alternative strategy for photoregulating catalytic reactivity. Instead of inducing conformational changes in a pre-existing catalyst, we harness light energy to construct an active catalyst *via* a photodimerization process. The [2 + 2] cycloaddition reaction—a widely studied photochemical process—forms cyclobutane adducts upon irradiation across a broad wavelength range[37] and has been investigated in cinnamic acid,[38] thymine,[39] coumarin, stilbene,[40] and, more recently, acrydylpyrene derivatives. Acrydylpyrene offers unique advantages as one of the mildest and most orthogonal photochemical systems, with wavelengths for self-dimerization and cycloreversion at approximately 435 nm and 330 nm, respectively. These reversible photodimerization processes have been applied to polymer ligation,[41–46] photodynamic hydrogels,[47–49] and the photocontrol of duplex formation between artificial nucleic acids and RNA.[50]

Here, we equipped an acrylamidylpyrene chromophore with a 1,4,7-triazacyclononane (TACN)·Zn(II) unit (Fig. 1), a moiety known to enhance catalytic activity in transphosphorylation reactions[51] by promoting cooperative effects between neighbouring TACN·Zn(II) units.[52–57] We demonstrated that irradiation at 420 nm induces both the *E*-to-*Z* isomerisation of the monomer, which did not affect the catalysis, and photodimerization into a catalytically active cyclobutane derivative. Prolonging the irradiation shifts the equilibrium towards the active dimer and the catalytic activity is reversibly regulated by alternating between 420 nm and 311 nm irradiation, which instead causes dissociation of the catalyst. Remarkably, the [2 + 2] cycloaddition is highly stereoselective, yielding a single cyclobutane product out of 11 theoretically possible regioisomers.

Results and discussion

After having synthesised the acrylamidylpyrene derivative ***E*-1·Zn(II)** (for details see SI, Section 2) we initially studied its

Dipartimento di Scienze Chimiche, Università degli studi di Padova, via Marzolo 1, 35131 Padova, Italy. E-mail: luca.gabrielli@unipd.it

© 2025 The Author(s). Published by the Royal Society of Chemistry

Open Access Article. Published on 29 August 2025. Downloaded on 10/28/2025 1:59:05 PM.
This article is licensed under a Creative Commons Attribution-NonCommercial 3.0 Unported Licence.

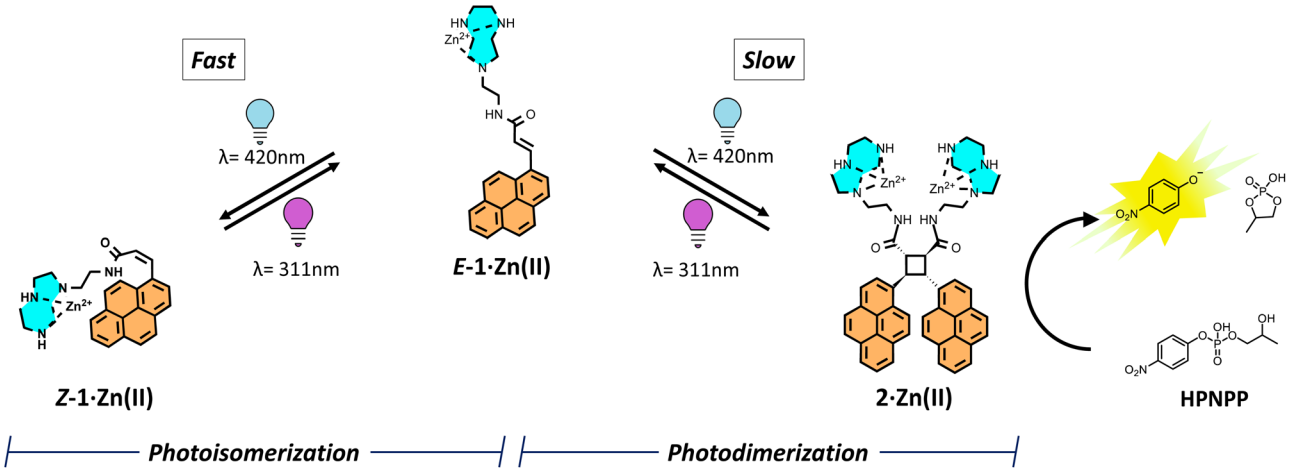

Fig. 1 Reaction scheme highlighting the studied processes: upon irradiation at 420 nm the *E*-1·Zn(II) monomer can isomerize into *Z*-1·Zn(II) (fast) or dimerize to give 2·Zn(II) (slow). The formed photodimer can catalyze the transphosphorylation of HPNPP into *p*-nitrophenol (PNP) and cyclic phosphate. The photoinduced processes can be reverted by irradiating with a wavelength of 311 nm.

photochemical behavior *via* ^{1}H-NMR spectroscopy, using D_2O : DMSO 8 : 2 as the solvent mixture, in order to prevent potential aggregation. The first process that we observed when irradiating a 0.5 mM solution of ***E*-1·Zn(II)** at 420 nm for 3 min was the photoisomerization from the *E* to the *Z* isomer, reaching around 85% of the *Z*-isomer at the photostationary state (Fig. 2b, c and S28; for details on the choice of wavelengths see SI, Section 3.3). Upon irradiation at 311 nm for 2 hours reversible photoisomerization from *Z* into *E* isomer took place, and this process could be repeated for different cycles. However, it was observed that the total concentration of monomers was slowly decreasing because of the formation of photodimer **2·Zn(II)** (Fig. S29 and S30).

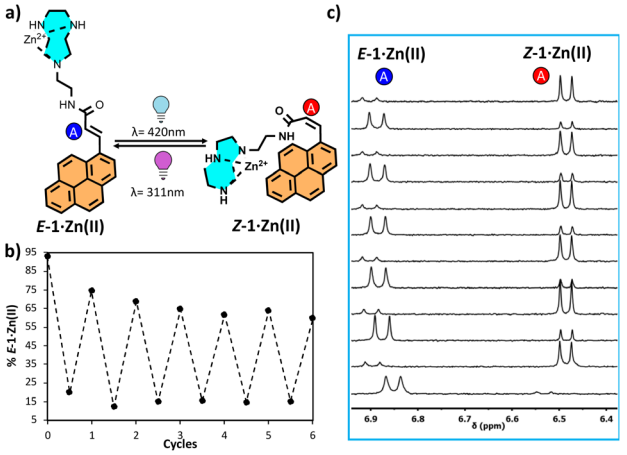

Fig. 2 (a) Reaction scheme of the reversible photoisomerization between *E*-1·Zn(II) and *Z*-1·Zn(II). (b) Graph showing the percentage of *E*-1·Zn(II) isomer as a function of the isomerization cycles (420/311 nm) and (c) corresponding ^{1}H-NMR highlighting the doublet typical of the *E* and *Z* isomers. The coupling constants J^2 of the olefinic protons signals are consistent with the *E* and *Z* isomers (respectively 16 Hz (6.9 ppm) and 12 Hz (6.5 ppm), see S28). The concentration-dependent variation in the chemical shift of the doublets arising from proton A of 1·Zn(II) suggests the presence of weak intermolecular interactions involving mainly the *E* isomer-at least to some extent.

In fact, when a 0.5 mM solution of ***E*-1·Zn(II)** in D_2O : DMSO 8 : 2 was irradiated for about 120 min at 420 nm, we observed that the [2 + 2] cycloaddition prevailed over the photoisomerisation process (92% of dimer), which was confirmed by mass spectrometry and ^{1}H-NMR spectroscopy (see S23–S27 and S33–S34), that showed the disappearance of the olefinic doublets at 7.6 ppm and 6.5 ppm and the appearance of two multiplets at 5.1 ppm and 3.9 ppm, consistent with the cyclobutane ring formation (Fig. 3a) of just a single regioisomer (see below).[58] Additionally, ^{1}H-NMR analysis revealed significant upfield shifts of the TACN protons upon photodimerization (Fig. 3a, red squares), consistent with a closer proximity to the pyrene ring in the cyclobutane structure. COSY and HSQC experiments (see Fig. S26 and S27) further confirmed the splitting of TACN CH_2 protons into two populations, indicating magnetic anisotropy effects from the pyrene ring.[59] The UV-vis spectra (Fig. 3c) showed that the characteristic absorption band of the conjugated ***E*-1·Zn(II)** (λ_{max} = 372 nm) undergoes a hypochromic shift in the isomer ***Z*-1·Zn(II)** (λ_{max} = 350 nm), which is replaced by the typical structured absorption band of non-conjugated pyrene in the photodimer **2·Zn(II)** (λ_{max} = 269, 279, 334 and 350 nm). This behaviour is fully consistent with the successful [2 + 2] cycloaddition.[44,60,61] The mismatch between the monomer absorption maximum (375 nm) and the red-shifted photodimerization wavelength (420 nm) also aligns well with earlier findings.[62–65] Reversibility of the dimerization can be achieved by irradiating the dimer solution at 311 nm (Fig. 3b and d). However, photodegradation hinders complete reversibility of the process (see S31 and S32), which regrettably occurs even increasing the irradiation wavelength to 365 nm.

We then decided to elucidate the structure of the obtained photodimer **2·Zn(II)**. The [2 + 2] cycloaddition of acrylamidylpyrene can theoretically result in 11 different regioisomers (see Table S1 for details), depending on the nature of

Open Access Article. Published on 29 August 2025. Downloaded on 10/28/2025 1:59:05 PM.
This article is licensed under a Creative Commons Attribution-NonCommercial 3.0 Unported Licence.

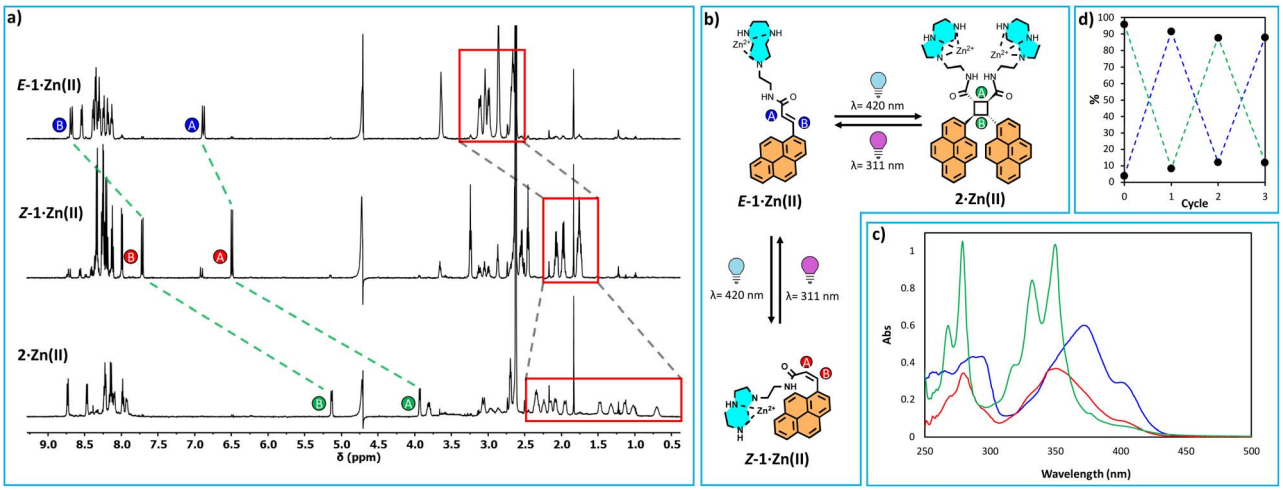

Fig. 3 (a) Comparison between ^{1}H-NMR of ***E*-1·Zn(II)**, ***Z*-1·Zn(II)** and **2·Zn(II)**; the styryl and the corresponding cyclobutane protons are highlighted with orange and green dots, while the CH_2 TACN·Zn(II) protons are highlighted with red squares. (b) Reaction scheme showing the reversible photoisomerization and photodimerization processes. (c) Comparison between UV-vis spectra of 20 μM water solutions of ***E*-1·Zn(II)** (blue), ***Z*-1·Zn(II)** (red) and **2·Zn(II)** (green). (d) Graph showing the percentage of ***E*-1·Zn(II)** (blue) and **2·Zn(II)** (green) as a function of the irradiation cycles (420/311 nm) for a 0.5 mM solution of ***E*-1·Zn(II)** in D_2O : DMSO-*d*6 8 : 2.

the reactive monomers (*E* and/or *Z*) and on their orientation (head/tail, and *syn*/*anti*). Given that the ^{1}H-NMR pattern of the cyclobutane protons signals are a fingerprint of the isomer, the initial focus for establishing the structure of the dimer was placed on the cyclobutane protons at 5.1 ppm and 3.9 ppm (Fig. S47). The observed multiplet pattern, consistent with an AA′BB′ spin system, was in agreement with a cyclobutane ring exhibiting C_2 symmetry.[66–69] This reduced the pool of possible candidates to only two isomers obtained by the head-to- head cycloaddition of either two ***E*-1·Zn(II)** or two ***Z*-1·Zn(II)** molecules (respectively ***EE*-hh-anti** and ***ZZ*-hh-anti** in Fig. 4a). Notably, NOE experiments cannot discriminate between these two isomers, as the distances between the A/A′ and B/B′ proton pairs are nearly identical in both isomers (2.4 Å for ***ZZ*-hh-anti** and 2.5 Å for ***EE*-hh-anti**). To resolve this ambiguity, we examined the coupling constants within the AA′BB′ spin system.[69] Since sterically hindered substituents can alter the geometry and the coupling networks of the cyclobutane ring, we employed DFT calculations to predict the *J* couplings for the cyclobutane protons of the ***EE*-hh-anti** and ***ZZ*-hh-anti** photodimers.

The optimized geometries of ***EE*-hh-anti** and ***ZZ*-hh-anti** dimers (Fig. 4b) were employed to calculate the coupling constants of the cyclobutane protons (NMR data are summarized in Tables S2–S4).

Comparison of the experimental ^{1}H-NMR signal of the protons resonating at $\delta_{exp} = 5.2$ ppm with simulated patterns based on DFT-calculated *J* values revealed a clear match for the ***EE*-hh-anti** isomer, while significant deviations were observed for the ***ZZ*-hh-anti** isomer (Fig. 4c and see Section S5 for details). This indicated that the photodimerization proceeded *via* the [2 + 2] cycloaddition of two ***E*-1·Zn(II)** monomers, yielding the ***EE*-hh-anti** isomer as the single photoproduct (Fig. 4d).

Interestingly, the dimerizing monomer is the less concentrated species, as approximately 85% of the initial monomer has already isomerized to the *Z* form. Although 20% DMSO prevents large-scale aggregation (see S39), ^{1}H-NMR experiments suggest that weak intermolecular interactions between ***E*-1·Zn(II)** monomers may still occur (see Fig. 2). These interactions could contribute to the high photodimerization efficiency observed even at low concentrations of the *E*-isomer (see S42). Additionally, it is worth noting that the photoisomerization rate is

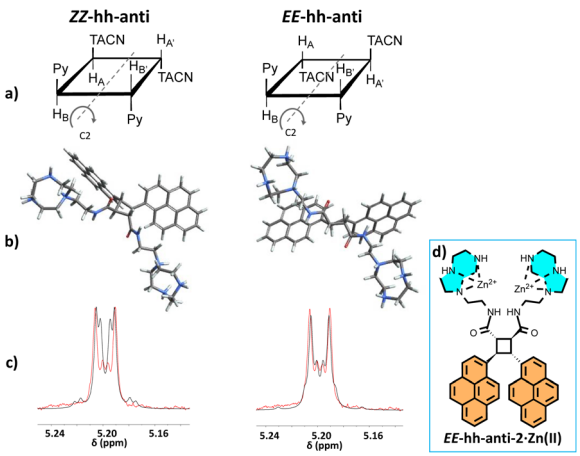

Fig. 4 (a) Schematic representations of the ***ZZ*-hh-anti** (left) and ***EE*-hh-anti** (right) isomers, with highlighted the C_2 symmetry axes. (b) Optimized structures of ***EE*-** and ***ZZ*-hh-anti** isomers. The cyclobutane ring protons of ***EE*-hh-anti** adopt quasi-*anti* conformations relative to each other, leading to relatively large ^3J couplings. Conversely, in ***ZZ*-hh-anti**, one proton pair features a dihedral angle close to 90°, typically associated with small ^3J couplings. (c) Overlap between experimental ^{1}H-NMR spectrum (red traces) and the simulated spectra from DFT-calculated NMR parameters for ***EE*-** and ***ZZ*-hh-anti** (black traces). The chemical shifts of calculated spectra were aligned to the experimental value of 5.20 ppm. (d) Molecular structures of the obtained ***EE*-hh-*anti*-2·Zn(II)** photodimer.

 © 2025 The Author(s). Published by the Royal Society of Chemistry

Open Access Article. Published on 29 August 2025. Downloaded on 10/28/2025 1:59:05 PM.
This article is licensed under a Creative Commons Attribution-NonCommercial 3.0 Unported Licence.

significantly faster than the photodimerization rate, allowing rapid *Z*-to-*E* isomerization to replenish the ***E*-1·Zn(II)** species as it is consumed during photodimerization.

After having established the molecular structure of the photodimer **2·Zn(II)**, we explored the catalytic properties of the system in the monomeric and dimeric states. The aim was to determine whether the photodimerization process enhances the system's catalytic activity toward the transphosphorylation reaction of 2-hydroxypropyl-4-nitrophenylphosphate (HPNPP), which is a model substrate for RNA (Fig. 5a). Hence, the formation of *p*-nitrophenol (PNP) from a 1 mM solution of HPNPP was followed *via* UV/vis spectroscopy, in the presence of the monomers ***E*-1·Zn(II)** and ***Z*-1·Zn(II)** (100 μM), or 50 μM of the photodimer **2·Zn(II)**. These experiments (Fig. 5 and Section 4 of the SI) showed that the *E*–*Z* photoisomerization of **1·Zn(II)** did not significantly affect the initial rate of the transphosphorylation (0.75 mM h^{-1} for ***E*-1·Zn(II)** and 0.93 mM h^{-1} for ***Z*-1·Zn(II)**), but that the clustering of two TACN·Zn(II) units in **2·Zn(II)** caused by photodimerization led to a 6-fold increase of the catalytic activity (4.22 mM h^{-1} for **2·Zn(II)**). The observed rate acceleration enhancement aligns with similar molecular systems containing two or more proximal TACN·Zn(II) units.[70–72]

One of the most attractive features of the use of light for tuning the catalytic properties is the possibility to temporally control a chemical reaction.[73] Thus, because of the significant difference in catalysis between monomers and dimer, we decided to study how the catalytic activity varies depending on the irradiation time. We observed that the presence of HPNPP and the resulting nitrophenolate anion interfered with the photodimerization process. To circumvent this practical limitation of the model substrate and to maintain precise control over the photochemical step, we decoupled catalyst irradiation from substrate conversion.[74] This approach allowed us to conceptually investigate whether irradiation time can effectively regulate catalytic activity. Aliquots were taken after different irradiation times and studied by ^{1}H-NMR spectroscopy to determine the mixture composition and by UV-vis spectroscopy to determine the catalytic activity. In particular, a solution of ***E*-1·Zn(II)** was irradiated at 420 nm to form the [2 + 2] cycloadduct,

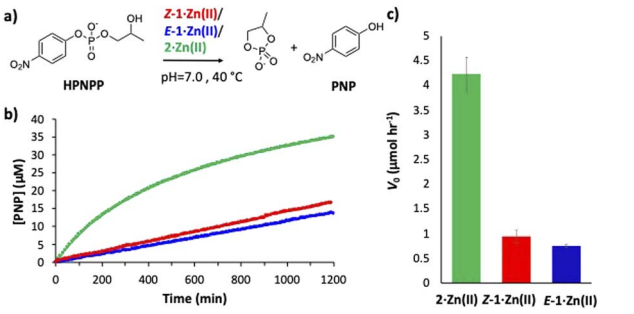

Fig. 5 (a) Reaction scheme of the studied HPNPP transesterification. (b) Concentration of the formed PNP as a function of the reaction time for a pH 7 solution of HPNPP 1 mM at 40 °C, in the presence of: ***E*-1·Zn(II)** (100 μM, blue line), or ***Z*-1·Zn(II)** (100 μM, red line), or **2·Zn(II)** (50 mM, green line). (c) Graph highlighting the observed initial reaction rates.

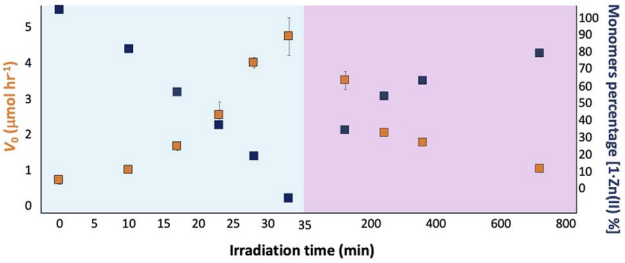

Fig. 6 Temporal control of HPNPP transesterification through photodimerization. The initial reaction rate of HPNPP transesterification (orange squares) and the percentage of monomers (**1·Zn(II)**, blue squares) are shown as a function of the irradiation time. In particular, a 1 mM solution of ***E*-1·Zn(II)** was initially irradiated at 420 nm for 35 minutes (green background), and then at 311 nm for 700 minutes (pink background). Over the time, this solution was analysed *via* ^{1}H-NMR and aliquots (corresponding to 50 μM of **1·Zn(II)**) were added to 1 mM HPNPP solutions, pH 7.0, 40 °C. The formation of PNP was followed *via* UV spectroscopy.

and the catalytic activity at different irradiation times was studied by taking 5 different aliquots of the irradiated mixture and adding these to a 1 mM HPNPP solution (Fig. 6, 0–35 minutes). In these experiments the irradiated ***E*-1·Zn(II)** solution was 1 mM instead of 0.5 mM (see Fig. 2 and 3), leading to a faster dimerization rate. Consequently, complete dimerization was achieved in just 33 minutes, and the irradiated wavelength was set to 311 nm to cause the dissociation of the photodimer **2·Zn(II)**. At 4 different times aliquots of the solution were taken and added to a 1 mM HPNPP solution. The initial rates of transesterification reaction were measured and plotted as a function of the irradiation time (Fig. 6, 0–800 minutes). The irradiation at 420 nm of a ***E*-1·Zn(II)** increased the transesterification rate of HPNPP about 6-fold, reaching the maximum after 33 minutes. This timing well correlates with the dimer formation rate, which indeed reaches the highest concentration after 33 minutes of irradiation (see also Fig. S43 and S44). On the other hand, subsequent irradiation at 311 nm caused a decrease in the reaction rate, which returned to initial values after around 700 minutes. Also, this trend well corresponds with the slower kinetic of the monomerization reaction, in fact 700 min of irradiation are needed to decrease the dimer concentration to 21%.

Conclusions

While photoisomerization processes are extensively explored for controlling system reactivity, the use of photodimerization reactions for this purpose remains largely unexplored. Here, we have described a styrylpyrene-based molecular system equipped with a TACN·Zn(II) catalytic unit that undergoes regioselective [2 + 2] cycloaddition upon visible light irradiation (420 nm). In addition to photodimerization, we observed *E*-to-*Z* photoisomerization, which does not hinder the process as prolonged irradiation drives the equilibrium toward the dimeric state. Even if photodegradation affects the efficiency, both the photoinduced processes are reversible, with irradiation at 311 nm restoring the original *E* isomer.

Open Access Article. Published on 29 August 2025. Downloaded on 10/28/2025 1:59:05 PM.
This article is licensed under a Creative Commons Attribution-NonCommercial 3.0 Unported Licence.

Remarkably, the photodimerization is highly regioselective, yielding only one photoisomer. Detailed ^{1}H-NMR spectral analysis, supported by DFT-calculations, confirmed the photodimer's *EE*-hh-anti geometry. Investigating the catalytic properties of this dimer toward HPNPP transesterification revealed a significant finding: while photoisomerization has no impact on catalysis, the [2 + 2] cycloaddition creates a dimer whose clustered catalytic units result in a 6-fold enhancement of the reaction rate compared to the monomeric system.

These results illustrate the potential of visible light to drive the covalent assembly of catalytically active molecules, enabling temporal control over system reactivity. Remarkably, while many photoswitches suffer from the thermodynamic instability of their active form, the catalytically active photodimer is a robust product that does not spontaneously revert to its monomeric inactive state. By establishing photodimerization as a viable alternative to photoisomerization for regulating catalysis, this work opens new avenues for designing light-responsive networks and advancing temporal reaction control strategies.

Author contributions

The manuscript was written through contributions of all authors. T. M., A. N. and M. L. performed the synthesis, the NMR and UV-vis spectroscopic experiments. F. R. performed DFT calculation and NMR simulation. S. B. UV-vis experiments and review, LP writing – review & editing. L. G. designed the project, analysed the data, supervised the research and wrote the manuscript.

Conflicts of interest

There are no conflicts to declare.

Data availability

The data supporting this article have been included as part of the SI, including the synthetic procedures and the characterizations of all products reported in this study. Details on photoreactivity studies and DFT calculations are included as well. See DOI: **https://doi.org/10.1039/d5sc03858h**.

Acknowledgements

LG thanks Italian Ministry of Education and Research (MUR, grant "Nanotune" 20227MP3CW) for funding, Ileana Menegazzo for assistance with NMR experiments and Ilaria Fortunati for assistance with spectroscopic measurements.

Notes and references

1 T. Ebrey and Y. Koutalos, Vertebrate Photoreceptors, *Prog. Retinal Eye Res.*, 2001, **20**, 49–94.
2 D. F. O'Brien, The Chemistry of Vision, *Science*, 1982, **218**, 1134–1138.
3 Q. Wang, Z. Zuo, X. Wang, L. Gu, T. Yoshizumi, Z. Yang, L. Yang, Q. Liu, W. Liu, Y.-J. Han, J.-I. Kim, B. Liu, J. A. Wohlschlegel, M. Matsui, Y. Oka and C. Lin, Photoactivation and Inactivation of Arabidopsis Cryptochrome 2, *Science*, 2016, **354**, 343–347.
4 J. I. Spiltoir and C. L. Tucker, Photodimerization Systems for Regulating Protein–Protein Interactions with Light, *Curr. Opin. Struct. Biol.*, 2019, **1**, 1–8.
5 Q. Wang, Q. Liu, X. Wang, Z. Zuo, Y. Oka and C. Lin, New Insights into the Mechanisms of Phytochrome–Cryptochrome Coaction, *New Phytol.*, 2018, **217**, 547–551.
6 A. Sgarbossa, G. Checcucci and F. Lenci, Photoreception and Photomovements of Microorganisms, *Photochem. Photobiol. Sci.*, 2002, **1**, 459–467.
7 Y.-J. Han, P.-Y. Song and J.-I. Kim, Phytochrome-Mediated Photomorphogenesis in Plants, *J. Plant Biol.*, 2007, **50**, 230–240.
8 V. Blanco, D. A. Leigh and V. Marcos, Artificial Switchable Catalysts, *Chem. Soc. Rev.*, 2015, **44**, 5341–5370.
9 M. Vlatkovic, L. Bernardi, E. Otten and B. L. Feringa, Dual Stereocontrol over the Henry Reaction Using a Light- and Heat-Triggered Organocatalyst, *Chem. Commun.*, 2014, **50**, 7773–7775.
10 D. Sud, T. B. Norsten and N. R. Branda, Photoswitching of Stereoselectivity in Catalysis Using a Copper Dithienylethene Complex, *Angew. Chem., Int. Ed.*, 2005, **44**, 2019–2021.
11 Z. S. Kean, S. Akbulatov, Y. Tian, R. A. Widenhoefer, R. Boulatov and S. L. Craig, Photomechanical Actuation of Ligand Geometry in Enantioselective Catalysis, *Angew. Chem., Int. Ed.*, 2014, **126**, 14736–14739.
12 T. Imahori, R. Yamaguchi and S. Kurihara, Azobenzene-Tethered Bis(Trityl Alcohol) as a Photoswitchable Cooperative Acid Catalyst for Morita–Baylis–Hillman Reactions, *Chem.–Eur. J.*, 2012, **18**, 10802–10807.
13 D. Wilson and N. R. Branda, Turning "on" and "off" a Pyridoxal 5′-Phosphate Mimic Using Light, *Angew. Chem., Int. Ed.*, 2012, **51**, 5431–5434.
14 M. Samanta, V. S. R. Krishna and S. Bandyopadhyay, A Photoresponsive Glycosidase Mimic, *Chem. Commun.*, 2014, **50**, 10577–10579.
15 R. Cacciapaglia, S. Di Stefano and L. Mandolini, The Bis-Barium Complex of a Butterfly Crown Ether as a Phototunable Supramolecular Catalyst, *J. Am. Chem. Soc.*, 2003, **125**, 2224–2227.
16 F. Würthner and J. Rebek, Photoresponsive Synthetic Receptors: Binding Properties and Photocontrol of Catalytic Activity, *J. Chem. Soc., Perkin Trans. 1*, 1995, 1727–1734.
17 D. Zhao, T. M. Neubauer and B. L. Feringa, Dynamic Control of Chirality in Phosphine Ligands for Enantioselective Catalysis, *Nat. Commun.*, 2015, **6**, 1–7.
18 B. M. Neilson and C. W. Bielawski, Photoswitchable Metal-Mediated Catalysis: Remotely Tuned Alkene and Alkyne Hydroborations, *Organometallics*, 2013, **32**, 3121–3128.
19 B. M. Neilson and C. W. Bielawski, Photoswitchable NHC-Promoted Ring-Opening Polymerizations, *Chem. Commun.*, 2013, **49**, 5453–5455.

 © 2025 The Author(s). Published by the Royal Society of Chemistry

Open Access Article. Published on 29 August 2025. Downloaded on 10/28/2025 1:59:05 PM.
This article is licensed under a Creative Commons Attribution-NonCommercial 3.0 Unported Licence.

20 B. M. Neilson and C. W. Bielawski, Photoswitchable Organocatalysis: Using Light to Modulate the Catalytic Activities of N-Heterocyclic Carbenes, *J. Am. Chem. Soc.*, 2012, **134**, 12693–12699.
21 T. Niazov, B. Shlyahovsky and I. Willner, Photoswitchable Electrocatalysis and Catalyzed Chemiluminescence Using Photoisomerizable Monolayer-Functionalized Surfaces and Pt Nanoparticles, *J. Am. Chem. Soc.*, 2007, **129**, 6374–6375.
22 Z. Chu, Y. Han, T. Bian, S. De, P. Kràl and R. Klajn, Supramolecular Control of Azobenzene Switching on Nanoparticles, *J. Am. Chem. Soc.*, 2019, **141**, 1949–1960.
23 G. De Bo, D. A. Leigh, C. T. McTernan and S. Wang, A complementary pair of enantioselective switchable organocatalysts, *Chem. Sci.*, 2017, **8**, 7077–7081.
24 L. Osorio-Planes, C. Rodríguez-Escrich and M. A. Pericàs, Photoswitchable Thioureas for the External Manipulation of Catalytic Activity, *Org. Lett.*, 2014, **16**, 1704–1707.
25 R. S. Stoll, M. V. Peters, A. Kuhn, S. Heiles, R. Goddard, M. Bühl, C. M. Thiele and S. Hecht, Photoswitchable Catalysts: Correlating Structure and Conformational Dynamics with Reactivity by a Combined Experimental and Computational Approach, *J. Am. Chem. Soc.*, 2009, **131**, 357–367.
26 Y. Wei, S. Han, J. Kim, S. Soh and G. A. Grzybowski, Photoswitchable Catalysis Mediated by Dynamic Aggregation of Nanoparticles, *J. Am. Chem. Soc.*, 2010, **132**, 11018–11102.
27 C. Z. J. Ren, P. Solís Muñana, J. Dupont, S. S. Zhou and J. L. Y. Chen, Reversible Formation of a Light-Responsive Catalyst by Utilizing Intermolecular Cooperative Effects, *Angew. Chem., Int. Ed.*, 2019, **58**, 15254–15258.
28 Y. Lee, A. Fracassi and N. K. Devaraj, Light-Driven Membrane Assembly, Shape-Shifting, and Tissue Formation in Chemically Responsive Synthetic Cells, *J. Am. Chem. Soc.*, 2023, **45**, 25815–25823.
29 M. Vlatkovic, L. Bernardi, E. Otten and B. L. Feringa, Dual Stereocontrol over the Henry Reaction Using a Light- and Heat-Triggered Organocatalyst, *Chem. Commun.*, 2014, **50**, 7773–7775.
30 R. Dorel and B. L. Feringa, Stereodivergent Anion Binding Catalysis with Molecular Motors, *Angew. Chem., Int. Ed.*, 2020, **132**, 795–799.
31 J. Wang and B. L. Feringa, Dynamic Control of Chiral Space in a Catalytic Asymmetric Reaction Using a Molecular Motor, *Science*, 2011, **331**, 1429–1433.
32 D. Wilson and N. R. Branda, Turning "on" and "off" a Pyridoxal 5′-Phosphate Mimic Using Light, *Angew. Chem., Int. Ed.*, 2012, **51**, 5431–5434.
33 B. M. Neilson and C. W. Bielawski, Photoswitchable Organocatalysis: Using Light to Modulate the Catalytic Activities of N-Heterocyclic Carbenes, *J. Am. Chem. Soc.*, 2012, **134**, 12693–12699.
34 B. M. Neilson and C. W. Bielawski, Photoswitchable Metal-Mediated Catalysis: Remotely Tuned Alkene and Alkyne Hydroborations, *Organometallics*, 2013, **32**, 3121–3128.
35 D. Sud, T. B. Norsten and N. R. Branda, Photoswitching of Stereoselectivity in Catalysis Using a Copper Dithienylethene Complex, *Angew. Chem., Int. Ed.*, 2005, **44**, 2019–2021.
36 T. Niazov, B. Shlyahovsky and I. Willner, Photoswitchable Electrocatalysis and Catalyzed Chemiluminescence Using Photoisomerizable Monolayer-Functionalized Surfaces and Pt Nanoparticles, *J. Am. Chem. Soc.*, 2007, **129**, 6374–6375.
37 G. Kaur, P. Johnston and K. Saito, Photo-Reversible Dimerisation Reactions and Their Applications in Polymeric Systems, *Polym. Chem.*, 2014, **5**, 2171–2186.
38 W. G. Kim, Photocure Properties of High-Heat-Resistant Photoreactive Polymers with Cinnamate Groups, *J. Appl. Polym. Sci.*, 2008, **107**, 3615–3624.
39 M. Jaljli Moghaddam, S. Hozumi, Y. Inaki and K. Takemoto, Functional Monomers and Polymers 159 Synthesis and Photochemical Reactions of Polymers Containing Thymine Photodimer Units in the Main Chain, *J. Polym. Sci., Part A: Polym. Chem.*, 1988, **26**, 3297–3308.
40 A. P. Somlai, R. A. Cozad, K. A. Page, H. R. Williams, D. Creed and C. E. Hoyle, The Photochemistry of Some Main Chain Liquid Crystalline 4,4′-Stilbene Dicarboxylate Polyesters, *Photochem. Photobiol. Sci.*, 2008, **7**, 578–587.
41 H. Frisch, F. R. Bloesser and C. Barner-Kowollik, Controlling Chain Coupling and Single-Chain Ligation by Two Colours of Visible Light, *Angew. Chem., Int. Ed.*, 2019, **131**, 3642–3648.
42 M. Liu, W. Wenzel and H. Frisch, Photocycloreversions within Single Polymer Chains, *Polym. Chem.*, 2020, **11**, 6616–6623.
43 D. E. Marschner, C. O. Franck, D. Abt, H. Mutlu and C. Barner-Kowollik, Fully Independent Photochemical Reactivity in One Molecule, *Chem. Commun.*, 2019, **55**, 9877–9880.
44 D. E. Marschner, H. Frisch, J. T. Offenloch, B. T. Tuten, C. R. Becer, A. Walther, A. S. Goldmann, P. Tzvetkova and C. Barner-Kowollik, Visible Light [2 + 2] Cycloadditions for Reversible Polymer Ligation, *Macromolecules*, 2018, **51**, 3802–3807.
45 H. Frisch, K. Mundsinger, B. L. J. Poad, S. J. Blanksby and C. Barner-Kowollik, Wavelength-Gated Photoreversible Polymerization and Topology Control, *Chem. Sci.*, 2020, **11**, 2834–2842.
46 X. Yi Oh, Q. Vu Thi, M. Mei Ling Yu, M. Izadyar, S. Ali Abbas Abedi, X. Liu and V. X. Truong, Moisture Tolerance, Thermally Stable and Light Switchable Adhesives Platform Based on Reversible Redshifted [2 + 2] Photocycloaddition, *Adv. Funct. Mater.*, 2025, 2421823.
47 V. X. Truong, F. Li, F. Ercole and J. S. Forsythe, Wavelength-Selective Coupling and Decoupling of Polymer Chains *via* Reversible [2 + 2] Photocycloaddition of Styrylpyrene for Construction of Cytocompatible Photodynamic Hydrogels, *ACS Macro Lett.*, 2018, **7**, 464–469.
48 K. Kalayci, H. Frisch, C. Barner-Kowollik and V. X. Truong, Wavelength-Dependent Stiffening of Hydrogel Matrices *via* Redshifted [2 + 2] Photocycloadditions, *Adv. Funct. Mater.*, 2020, **30**, 1908171.
49 V. X. Truong, J. Bachmann, A. N. Unterreiner, J. P. Blinco and C. Barner-Kowollik, Wavelength-orthogonal stiffening of hydrogel networks with visible light, *Angew. Chem., Int. Ed.*, 2022, **61**, e202113076.

Open Access Article. Published on 29 August 2025. Downloaded on 10/28/2025 1:59:05 PM.
This article is licensed under a Creative Commons Attribution-NonCommercial 3.0 Unported Licence.

50 K. Murayama, Y. Yamano and H. Asanuma, *J. Am. Chem. Soc.*, 2019, **141**, 9485–9489.
51 P. Solís Muñana, G. Ragazzon, J. Dupont, C. Z.-J. Ren, L. J. Prins and J. L.-Y. Chen, Substrate-Induced Self-Assembly of Cooperative Catalysts, *Angew. Chem., Int. Ed.*, 2018, **130**, 16707–16712.
52 C. Pezzato, J. L. Y. Chen, P. Galzerano, M. Salvi and L. J. Prins, Catalytic Signal Amplification for the Discrimination of ATP and ADP Using Functionalised Gold Nanoparticles, *Org. Biomol. Chem.*, 2016, **14**, 6811–6820.
53 S. Maiti, I. Fortunati, C. Ferrante, P. Scrimin and L. J. Prins, Dissipative Self-Assembly of Vesicular Nanoreactors, *Nat. Chem.*, 2016, **8**, 725–731.
54 L. Gabrielli, L. Goldin, S. Chandrabhas, A. Dalla Valle and L. J. Prins, Chemical Information Processing by a Responsive Chemical System, *J. Am. Chem. Soc.*, 2024, **146**, 2080–2088.
55 J. Czescik, Y. Lyu, S. Neuberg, P. Scrimin and F. Mancin, Host–Guest Allosteric Control of an Artificial Phosphatase, *J. Am. Chem. Soc.*, 2020, **142**, 6837–6841.
56 S. Chandrabhas, S. Maiti, I. Fortunati, C. Ferrante, L. Gabrielli and L. J. Prins, Nucleotide-Selective Templated Self-Assembly of Nanoreactors under Dissipative Conditions, *Angew. Chem., Int. Ed.*, 2020, **59**, 22223–22229.
57 G. Zaupa, C. Mora, R. Bonomi, L. J. Prins and P. Scrimin, Catalytic Self-Assembled Monolayers on Au Nanoparticles: The Source of Catalysis of a Transphosphorylation Reaction, *Chem.–Eur. J.*, 2011, **17**, 4879–4889.
58 The high regioselectivity observed is solvent-dependent. When photodimerization was carried out in D_2O, a minor amount of a second photodimer was detected (see Fig. S39 and S40).
59 A. Bugaut, J. J. Toulmé and B. Rayner, SELEX and Dynamic Combinatorial Chemistry Interplay for the Selection of Conjugated RNA Aptamers, *Org. Biomol. Chem.*, 2006, **4**, 4082–4088.
60 T. Doi, H. Kawai, K. Murayama, H. Kashida and H. Asanuma, Visible-Light-Triggered Cross-Linking of DNA Duplexes by Reversible [2 + 2] Photocycloaddition of Styrylpyrene, *Chem.–Eur. J.*, 2016, **22**, 10533–10538.
61 N. P. Kovalenko, A. Abdukadirov, V. I. Gerko and M. V. Alfimov, Some peculiarities of diarylethylenes with 3-pyrenyl fragments, *J. Appl. Spectrosc.*, 1980, **32**, 607–612.
62 D. E. Fast, A. Lauer, J. P. Menzel, A.-M. Kelterer, G. Gescheidt and C. Barner-Kowollik, Wavelength-dependent photochemistry of oxime ester photoinitiators, *Macromolecules*, 2017, **50**(5), 1815–1823.
63 I. M. Irshadeen, S. L. Walden, M. Wegener, V. X. Truong, H. Frisch, J. P. Blinco and C. Barner-Kowollik, Action plots in action: in-depth insights into photochemical reactivity, *J. Am. Chem. Soc.*, 2021, **143**, 21113–21126.
64 S. L. Walden, J. A. Carroll, A.-N. Unterreiner and C. Barner-Kowollik, Photochemical action plots reveal the fundamental mismatch between absorptivity and photochemical reactivity, *Adv. Sci.*, 2024, **11**, 2306014.
65 J. A. Carroll, F. Pashley-Johnson, M. Klein, T. Stephan, A. K. Pandey, M. Walter, A.-N. Unterreiner and C. Barner-Kowollik, Microenvironments Explain the Mismatch between Photochemical Absorptivity and Reactivity, *J. Am. Chem. Soc.*, 2025, **147**(30), 26643–26651.
66 G. Montaudo and S. Caccamese, Chalcone Photodimers and Related Compounds, *J. Org. Chem.*, 1970, **38**, 710–715.
67 J. Vansant, S. Toppet, G. Smets, J. P. Declercq, G. Germain and M. Van Meerssche, Azastilbene. 2. Photodimerisation, *J. Org. Chem.*, 1980, **45**, 1565–1573.
68 L. Paolillo, H. Ziffer and O. Buchardt, Nuclear Magnetic Resonance Analysis of Several Photodimers Containing a Cyclobutane Ring, *J. Org. Chem.*, 1970, **35**, 38–42.
69 M. Hesse, H. Meier and B. Zeeh, *Spectroscopic Methods in Organic Chemistry 2nd edition*, Thieme, New York, 2008, pp. 116–118.
70 A. Scarso, G. Zaupa, F. B. Houillon, L. J. Prins and P. Scrimin, Tripodal, cooperative, and allosteric transphosphorylation metallocatalysts, *J. Org. Chem.*, 2007, **72**, 376–385.
71 T. Marchetti, D. Frezzato, L. Gabrielli and L. J. Prins, ATP drives the formation of a catalytic hydrazone through an energy ratchet mechanism, *Angew. Chem., Int. Ed.*, 2023, **62**, e202307530.
72 E. S. Bencze, C. Zonta, F. Mancin, L. J. Prins and P. Scrimin, Distance between Metal Centres Affects Catalytic Efficiency of Dinuclear Co III Complexes in the Hydrolysis of a Phosphate Diester, *Eur. J. Org Chem.*, 2018, **39**, 5375–5381.
73 S. Aubert, M. Bezagu, A. C. Spivey and S. Arseniyadis, Spatial and Temporal Control of Chemical Processes, *Nat. Rev. Chem.*, 2019, **3**, 706–710.
74 S. Neri, S. G. Martin, C. Pezzato and L. J. Prins, Photoswitchable Catalysis by a Nanozyme Mediated by a Light-Sensitive Cofactor, *J. Am. Chem. Soc.*, 2017, **139**, 1794–1997.

 © 2025 The Author(s). Published by the Royal Society of Chemistry